Soils and Foundations 2014;54(1):45–55

The Japanese Geotechnical Society

Soils and Foundations

www.sciencedirect.com
journal homepage: www.elsevier.com/locate/sandf

Large-scale triaxial tests of dense gravel material at low confining pressures

Stanislav Lenart[a,b,*], Junichi Koseki[b], Yukika Miyashita[b], Takeshi Sato[c]

[a]*Slovenian National Building and Civil Engineering Institute (ZAG), Slovenia*
[b]*Institute of Industrial Science (IIS), The University of Tokyo, Japan*
[c]*Integrated Geotechnology Institute Ltd., Japan*

Received 28 August 2012; received in revised form 2 July 2013; accepted 24 July 2013
Available online 22 January 2014

Abstract

The results of a series of large-scale triaxial tests performed on dense, prismatic gravel specimens, with a height of 50 cm and a cross-section of 23 cm × 23 cm, are described. The specimens were prepared at a density equal to approximately 95% of the maximum density at the optimum moisture content. Deformations were measured locally using vertical and horizontal local deformation transducers. Stress conditions with selected levels of very low confining pressure were used to simulate specific conditions in the case of road and railway embankments. Particular attention was paid to the bedding error at the top and the bottom ends of the specimens, and to fixing transducers onto the membrane to be used under low confining pressure. The confining pressure was applied by vacuum and varied from 10 kPa to 75 kPa. Unsaturated specimens were tested under drained triaxial compression using monotonic and cyclic loading with frequencies in the range of 0.5–5 Hz. The effects of a large number of load cycles and of specimen preloading were investigated.

Keywords: Gravel; Large-scale triaxial test; Low confining pressure; Cyclic loading

1. Introduction

Gravel materials in flexible pavements play an essential role in the overall deformation behaviour of such pavements. The goal during the construction process is to compact the gravel material into a layer at the densest and stiffest possible state, which can be achieved by using the optimum moisture content defined by the Proctor compaction test. During the operation, the unbound gravel material layer is exposed to specific in situ stress conditions and traffic loads. These are simulated in laboratory tests to better understand the deformation behaviour of the gravel material.

Repeated load triaxial tests, with variable or constant confining pressure, have been used for more than one decade to evaluate the mechanical properties of unbound granular materials (Gomes-Correia et al., 1999). A standardized procedure (EN 13286-7) defines a test specimen with a diameter larger than 5 times the maximum particle size of the material, resulting usually in a diameter of 150 mm and a height of 300 mm (Erlingsson and Magnusdottir, 2002). In these tests the response is measured by displacement transducers attached directly to the central part of the specimen. The attachment is enabled by anchors which penetrate into the specimen. For this reason some local disturbance may be present in the specimen. No effort is made to reduce the bedding error due to friction between the specimen and the top cap or between the specimen and the pedestal.

*Corresponding author at: Slovenian National Building and Civil Engineering Institute (ZAG), Slovenia.
E-mail address: stanislav.lenart@zag.si (S. Lenart).
Peer review under responsibility of The Japanese Geotechnical Society.

Production and hosting by Elsevier

0038-0806
http://dx.doi.org/10.1016/j.sandf.2013.12.005

2. Stress conditions in railway roadbeds

The large-scale triaxial tests presented in this paper were conducted giving consideration to the results of practical applications in railway track design. Thus, tests were needed for which the in situ stress conditions and railway traffic loads could be adequately simulated.

Momoya et al. (2005) presented the load distribution under sleepers for moving-wheel loading and fixed-point loading. Following their procedure, Fig. 1 shows the results for a typical prototype railway track, with a distance between adjacent sleepers of 60 cm. A maximum axle load equal to 225 kN, as defined in the Slovenian regulations for railway design, was used in the analysis.

A noticeable difference between the peak vertical pressure levels under the sleepers, for moving-wheel loading and fixed-point loading, can be observed (Fig. 1). The stress conditions in the sub-ballast layer, approximately 50 cm under the sleepers, were calculated using the theory of elasticity (Poulos and Davis, 1974). As can be seen in Fig. 2, the maximum vertical stress does not exceed 150 kPa, whereas the horizontal stress lies in the range of 10–55 kPa. It should be noted that the possible effects of the principal stress axis rotation, induced by the non-zero values of shear stress τ_{zx} and investigated by Momoya et al. (2005) and Inam et al. (2012), among others, were out of the scope of the present study.

It is obvious that rather low confining pressure should be used in triaxial tests simulating in situ stress conditions. Large-scale triaxial tests on dense gravel material under cyclic loading were conducted in the past by other researchers (AnhDan and Koseki, 2004; Maqbool and Koseki, 2010, among others), but the confining pressure exceeded 50 kPa in most of the studies, except for a limited number of studies, such as Ezaoui et al. (2010), Taheri et al. (2012) and Taheri and Tatsuoka (2012).

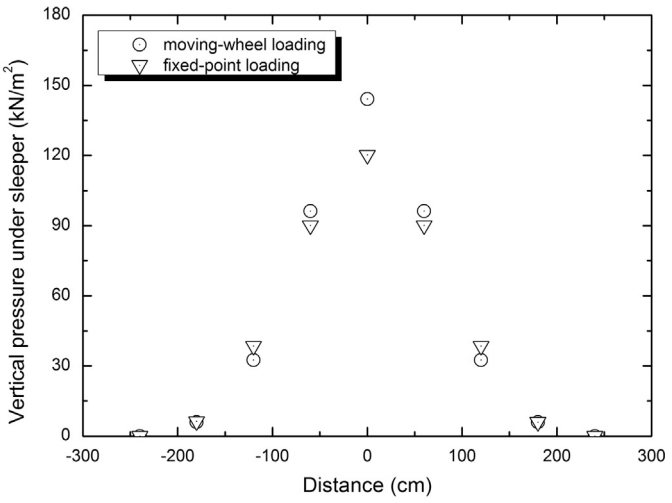

Fig. 1. Vertical pressure under sleepers at different distances from the loading point. The width of the sleepers is equal to 24 cm and the length is equal to 260 cm. (based on Momoya et al. (2005)).

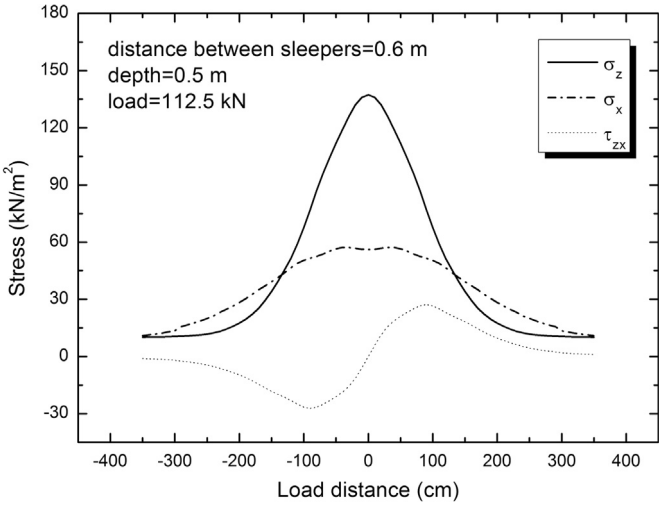

Fig. 2. Typical stress distribution under rail track.

3. Testing procedures

Considering the issues presented above, a different approach to dense gravel material deformation tests was used. The present research followed two main goals:

(1) to modify the existing testing apparatus in such a way that low confining pressure of the tested unbound gravel material could be used. Local disturbances (Erlingsson and Magnusdottir, 2002) due to the penetration of anchors at the side of the specimen and local confinement of the specimen caused by friction between the specimen and the top cap or the pedestal had to be avoided. The accuracy of the modified testing device needed to be assessed, and
(2) to investigate the effect of repeated loading on the unbound gravel material used for railway tracks.

Although the same large-scale triaxial apparatus had already been used in earlier research work (AnhDan et al., 2006a, 2006b), the tests presented in this paper differed from previous tests with respect to the low confining pressure applied (less than 50 kPa). They also differed in terms of the standardized procedure (EN 13286-7), namely, the elimination of local disturbances due to the penetration of the displacement transducer anchors into the specimen, as well as the bedding error.

3.1. Large-scale triaxial apparatus

The large-scale triaxial apparatus at the Institute of Industrial Science, University of Tokyo, was used. The device and its calibration have been described in detail in previous reports (e.g., Goto et al., 1991; Hoque et al., 1996; AnhDan and Koseki, 2004; AnhDan et al., 2006a, 2006b). The procedures described therein were used to calibrate the transducers. The test results were validated by test repetition. Although a major part of the testing device had been developed and verified earlier, two components still needed to be assessed. Firstly,

modification of pseudo-hinged attachments for operation under a low confining pressure environment had to be verified. This will be explained later in Section 4. Secondly, although the apparatus also consists of a pressure cell (see AnhDan et al., 2006a, 2006b), due to the low confining pressure used and in order to save electricity consumption, the confining pressure was applied by means of a partial vacuum, as back pressure. While the vacuum was applied at the bottom of the specimen, it was measured (controlled) at the top of the specimen.

A series of tests on prismatic specimens, 50 cm in height and 23 cm × 23 cm in cross-section, was conducted. The axial loading device employed an electro-hydraulic actuator with a capacity of 490 kN. The axial load was measured by means of a load cell attached to the top cap in order to eliminate the effects of the piston friction.

The axial strain (ε_1) was measured by three pairs of vertical local deformation transducers (LDTs) (Goto et al., 1991) placed at three heights on the specimen. One of the LDTs was combined with different types of attachments (to be described in more detail later in Section 4.2) by an extra pair of LDTs. The lateral strain (ε_3) was measured by another three pairs of horizontal LDTs, also placed at three heights on the specimen. The positions of all the LDTs and the test specimen before loading are shown in Fig. 3.

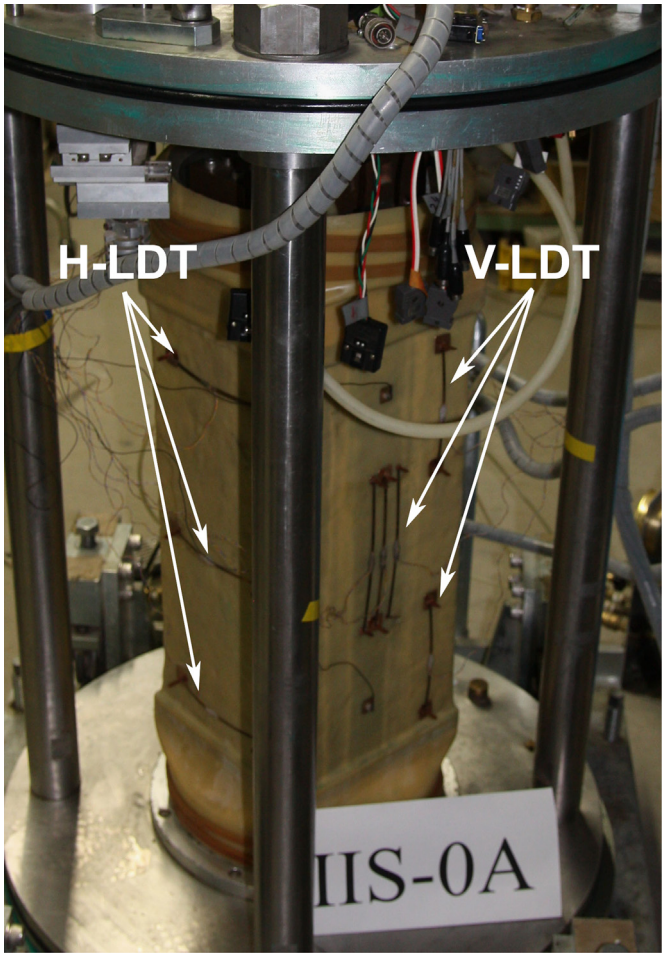

Fig. 3. Prismatic specimen in the large-scale triaxial apparatus.

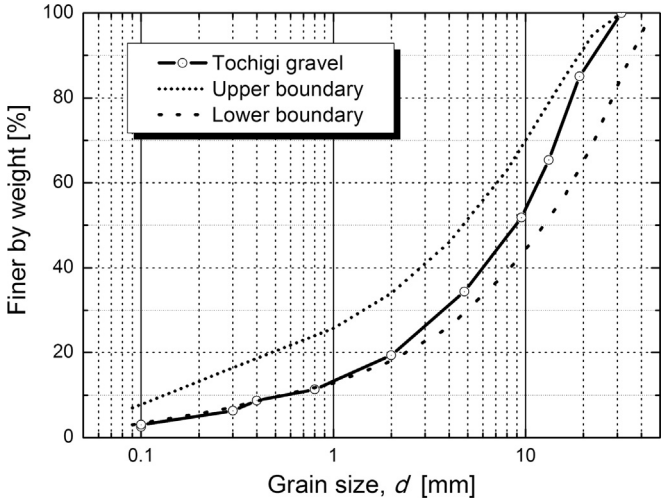

Fig. 4. Gradation curve of tested Tochigi gravel.

In order to reduce friction between the specimen and the rigid plates of the top cap and the pedestal, a lubrication layer was inserted between them. The recommendations of previous researchers (Goto et al., 1993; AnhDan and Koseki, 2004) were modified in such a way that one lubrication layer consisted of two 0.8-mm-thick rubber membranes and two 125-μm layers (equivalent to two layers of Scotch tape) of thick silicone grease. No correction for the effect of the membrane force was applied in the analysis of the test results.

3.2. Specimen preparation

The testing material was well-graded crushed stone, called Tochigi gravel. Its gradation is within the boundary gradation curves for the unbound granular base course material used in Slovenia (Fig. 4). It consists of angular to sub-angular particles with a coefficient of uniformity $C_u=32$ and a specific gravity $G_s=2.68$. The optimum moisture content and the maximum dry density were defined by a modified Proctor compaction test as $w_{opt}=4.0\%$ and $\rho_d=2.168$ g/cm^3, respectively.

Dense specimens were prepared by manual compaction by a falling hammer at a nearly optimum moisture content (Table 1). The specimens were compacted in 10 layers, each with a thickness of 5 cm. Before placing the material for the next layer, the surface of the previously compacted layer was scraped to a depth of about 2 cm to ensure good interlocking between the vertically adjacent layers. The compaction was applied for the purpose of obtaining a dry density of the specimen as close as possible to that defined as the optimum in the modified Proctor test. In reality, approximately 95% of the maximum density, on average, was reached.

3.3. Testing programme

The test results for four specimens are presented in this paper. The general testing programme is briefly described in Table 2. It consists of the initial isotropic consolidation of the specimens, and alternately monotonic and cyclic loading. The

Table 1
Details about specimens.

Specimen	IIS-0A	IIS-0C	IIS-0E	IIS-0F
Dry density (g/cm^3)	2.018	2.035	2.053	2.074
% of ρ_d by modified Proctor	93.1	93.9	94.7	95.7
Void ratio, (dimensionless)	0.33	0.32	0.31	0.29
Moisture content (%)	4.93	4.85	3.73	4.17

Table 2
Testing programme.

Loading condition	Test phases
Initial isotropic consolidation	1
Monotonic loading	2, 4, 6, 8, 10, 12, 14, 16
Cyclic loading	3, 5, 7, 9, 11, 13, 15

loading parameters used in the test are described in detail in Table 3.

Tests IIS-0A and IIS-0C were performed to verify the testing device modifications (e.g., local strain measurements and application of high frequency loading), whereas tests IIS-0E and IIS-0F were performed to investigate the effects of loading on unbound gravel material.

All the tests were drained triaxial compression tests conducted at a constant confining pressure σ_3 of 25 kPa. The exception was test IIS-0A (Fig. 5(a)), for which the confining pressure was, initially, 10 kPa (Phase 1). In this test, after applying large amplitude monotonic (Phase 2) and cyclic loading (Phase 3) in the vertical direction, isotropic consolidation to 15 kPa followed (Phase 4). Large amplitude cyclic loading was performed in Phase 5. A similar procedure was repeated in steps with confining pressure levels of 25, 50 and 75 kPa (Phases 6–11), as shown in the close-up view in Fig. 5(b). The test was continued by isotropic unloading to 10 kPa (Phase 12) and large amplitude cyclic loading (Phase 13). The loading was completed by monotonic loading to failure (Phase 16). Note that Phases 14 and 15 were not executed in test IIS-0A. The main purpose of this test was to study the effect of low confining pressure on the performance of the pseudo-hinge attachments of the LDTs. Details about the testing programme are presented in Table 2.

Except for test IIS-0A, during monotonic loading in all the tests at several stress states, many very small vertical unloading/reloading cycles were conducted for the purpose of evaluating the quasi-elastic properties. At the end of the series of small cycle loadings, the specimen was unloaded to a deviator stress of zero and then reloaded.

The aim of test IIS-0C (Fig. 6(a)) was to test the capability of the hydraulic actuator in the case of different loading frequencies. The specimen was initially isotropically consolidated to a confining pressure of 25 kPa (Phase 1), followed by monotonic loading in the vertical direction (Phase 2). The loading was stress-controlled with small strain cyclic loading at several stress states. Each of these stress states was followed by unloading to a deviator stress of zero, and then reloading was performed (Fig. 6(b)). Cyclic loading with gradually increasing loading frequencies and a different number of loading cycles was performed in Phases 3 ($f=0.5$ Hz), 5 ($f=1$ Hz), 7 ($f=3$ Hz) and 9 ($f=5$ Hz) without any monotonic loading in the intermediate phases. The specimen was exposed to a total of 20,000 load cycles in the first stage, completed with a frequency of 1 Hz (Phase 11) (Fig. 6(b)). Monotonic loading (Phase 12) and another 20,000 load cycles with a frequency of 0.5 Hz (Phase 13) followed. Monotonic loading (Phase 14) and cyclic loading (Phase 15) were repeated with a somewhat larger load amplitude and fewer load cycles. The test was completed with monotonic loading to failure (Phase 16).

As a reference case, the results from test IIS-0E are shown in Fig. 7. The main purpose of this test was to provide reference data about the stress–strain response for a specimen without exposure to preloading or a large number of cyclic loadings. The specimen was initially isotropically consolidated to a confining pressure of 25 kPa (Phase 1). Phase 2, using monotonic loading up to a deviator stress $q=\sigma_1-\sigma_3$ of 230 kPa, was stress-controlled with small strain cyclic loading at several stress states. Each of these stress states was followed by unloading to a deviator stress of zero and reloading. Phase 2 was followed directly by Phase 16, which consisted of strain-controlled monotonic loading up to failure.

In the case of test IIS-0F, the first monotonic loading up to $q=130$ kPa (Phase 2) was followed by 10,000 large-amplitude load cycles (Phase 3). The monotonic loading was repeated up to an increased deviator stress of $q=230$ kPa (Phase 4) and continued by cyclic loading with a progressively increasing deviator stress (Phases 5, 7, 9 and 11) up to $q=345$ kPa (Phase 13). During a total of 5000 load cycles, the accumulated strain increased progressively. One can observe in Fig. 8 the amount of strain accumulated during 40 load cycles at different loading amplitudes. The test was continued with stress-controlled (up to $q=250$ kPa) (Phase 14) monotonic loading, and was completed by strain-controlled monotonic loading (Phase 16) to failure. In order to simplify the picture, not all the load cycles during the cyclic loading with the same amplitude are shown in Figs. 6(a) and 8.

4. Assessment of testing accuracy due to the device modification

4.1. Hydraulic actuator capability

In test IIS-0C, the loading frequencies varied from 0.5 Hz up to 5 Hz. The primary aim was to investigate the hydraulic actuator's capability for higher frequency loading. It can be seen during the last cyclic loading ($N=500$), in Fig. 6, that the cyclic stress amplitude was initially smaller, and then increased. More than 200

Table 3
Testing parameters.

Test phase	Test no. and purpose of test			
	IIS-0A Effect of pseudo-hinge attachments of LDT	IIS-0C Effects of preloading, loading frequency, large number of load cycles	IIS-0E Reference case Monotonic loading, Effects of preloading	IIS-0F Effects of preloading,load amplitude increase, number of load cycles
1	$p'=10$ kPa	$p'=25$ kPa	$p'=25$ kPa	$p'=25$ kPa
2	$q=97$ kPa and unloading	$q=100$ kPa[a]	$q=230$ kPa[a]	$q=130$ kPa[a]
3	$q=30$–97 kPa, strain rate 0.1%/min, $N=10$ cycles	$q=0$–100 kPa, $f=0.5$ Hz, $N=1000$ cycles	–	$q=0$–130 kPa, $f=1.0$ Hz, $N=10{,}000$ cycles
4	$p'=15$ kPa[d]	–	–	$q=230$ kPa[a]
5	$q=30$–97 kPa, strain rate 0.1%/min, $N=10$ cycles	$q=10$–90 kPa, $f=1.0$ Hz, $N=1500$ cycles	–	$q=0$–210 kPa, $f=1.0$ Hz, $N=1000$ cycles
6	$p'=25$ kPa[d]	–	–	–
7	$q=30$–97 kPa, strain rate 0.1%/min, $N=10$ cycles	$q=30$–65 kPa, $f=3.0$ Hz, $N=7500$ cycles	–	$q=20$–240 kPa, $f=1.0$ Hz, $N=1000$ cycles
8	$p'=50$ kPa[d]	–	–	–
9	$q=30$–97 kPa, strain rate 0.1%/min, $N=3$ cycles	$q=35$–60 kPa, $f=5$ Hz, $N=9980$ cycles	–	$q=23$–278 kPa, $f=1.0$ Hz, $N=1000$ cycles
10	$p'=75$ kPa[d]	–	–	–
11	$q=30$–97 kPa, strain rate 0.1%/min, $N=5$ cycles	$q=0$–250 kPa, $f=1$ Hz, $N=20$ cycles	–	$q=23$–310 kPa, $f=1.0$ Hz, $N=1000$ cycles
12	$p'=10$ kPa[d]	$q=300$ kPa[a]	–	–
13	$q=30$–97 kPa, strain rate 0.1%/min, $N=5$ cycles	$q=10$–275 kPa, $f=0.5$ Hz, $N=20{,}000$ cycles	–	$q=30$–345 kPa, $f=1.0$ Hz, $N=1000$ cycles
14	–	$q=405$ kPa[a,b]	–	$q=250$ kPa[a]
15	–	$q=15$–310 kPa, $f=0.5$ Hz, $N=500$ cycles	–	–
16[c]	To failure ($q=207$ kPa)	To failure ($q=442$ kPa)	To failure ($q=344$ kPa)	To failure ($q=358$ kPa)

[a]At several stress states during monotonic triaxial compression, many very small vertical unload/reload cycles were conducted to evaluate the quasi-elastic properties. At the end of each small cycle loading, the specimen was unloaded to a zero deviatoric stress, and then reloaded.
[b]The monotonic loading was supposed to continue to $q>405$ kPa, but the deformation started to develop rapidly.
[c]Strain rate 0.11%/min.
[d]Isotropic.

load cycles were needed to achieve a constant loading amplitude. Fig. 9 presents typical stress–strain loops in Phases 3–9 with different loading frequencies. The hydraulic actuator was supposed to set a constant load amplitude (with a loading of $q=0$–100 kPa). It is clear, however, that the desired load amplitude was not achieved, particularly when the frequency was more than 1 Hz. Based on this observation, 1 Hz was chosen as the optimum frequency; it was used in all the other cyclic loading tests.

4.2. Local strain measurements

When measuring local strain in a triaxial specimen using LDTs, it is crucial to ensure their secure attachment to the specimen. Pseudo-hinged attachments, as described by Goto et al. (1991), were used in these tests. A contact force of 1.2–2.9 N acts at the hinges in the case of the dimensions of the LDTs used here. Due to the low confining pressure, attention must be paid to possible errors caused by the slippage or the rotation of the hinge and membrane according to the specimen′s deformation.

To solve this problem, the contact area between the hinge and the membrane was increased with an extra plate. As shown in Fig. 10, two dimensions of plates were used: 1-cm and 2-cm squares for LDTs A and B, respectively. LDT C was attached by a normal 5-mm hinge. When a confining pressure of 10 kPa is used, a 1-cm square plate is large enough to assure a balance of forces.

During the variation of confining pressure and the application of cyclic loads in test IIS-0A, the responses of different types of attachments were compared. Fig. 11(a) shows the response during one typical section of the test. There was no noticeable difference when the confining pressure was increased, whereas some errors occurred when the confining pressure was decreased. As it decreased from 75 kPa to 10 kPa, the extension was measured by an external LVDT (linear variable displacement transducer). The responses of LDTs A and C also exhibited some contraction. They included some errors due to their smaller plates for the hinges, if compared to the response of LDT B (2-cm plate). For this reason the latter type of attachment was chosen for the rest of the tests.

Fig. 11(b) compares the stress–strain relationship measured externally by the LVDT and locally by the LDTs with different types of attachments. During one cycle of large amplitude loading, there was almost no difference in the responses of the LDTs, whereas the external measurement showed noticeably lower stiffness due to the included bedding error.

4.3. Bedding error

As mentioned above, we tried to avoid the effect of disturbed zones forming at both ends of the specimen during testing. The use of double lubrication layers at both ends was

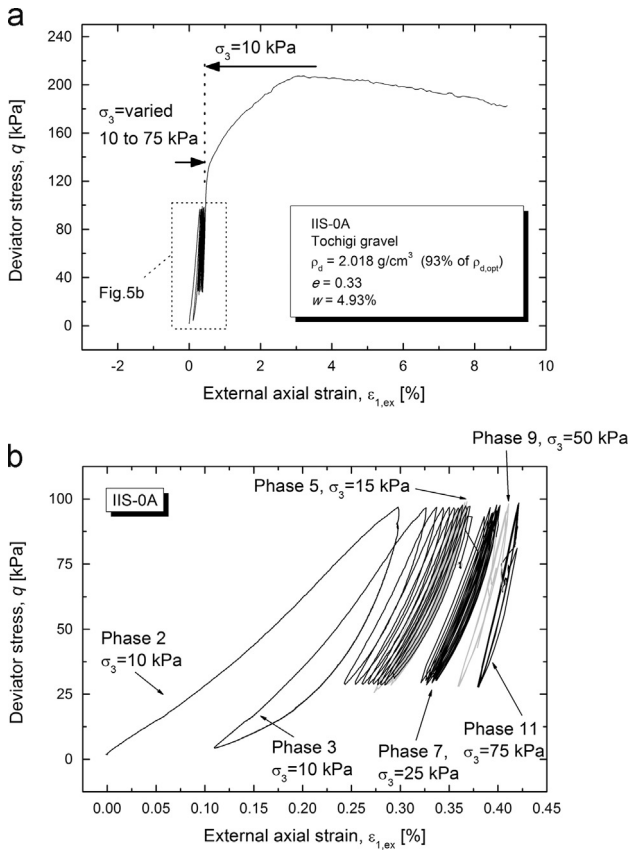

Fig. 5. (a) Overall axial stress–strain relationship and (b) its close-up view up to Phase 11, test IIS-0A.

designed to decrease the degree of confinement at the ends of the specimen.

Fig. 12 shows the average axial strain measured locally at the top and the bottom third of the specimen, as compared to the axial strain measured in the central part of the specimen. The axial strain in the centre and that at the bottom of the specimen are nearly identical to each other, suggesting homogeneity of the lower two thirds of the specimen and a good performance by the lubrication layer. The upper third of the specimen exhibits slightly larger strain, which was probably caused by insufficient compaction near the top of the specimen.

The impact of the bedding error on the strain measurements can also be observed if the strain measured externally (Fig. 5(b)) is compared to the strain measured locally (Fig. 13(a)).

5. Test results and discussions

5.1. Effect of confining pressure

The confining pressure was gradually increased in Phases 1–11 in test IIS-0A, in order to also evaluate the effect of low confining pressure on the deformation properties of dense gravel material. Fig. 13 presents a close-up view of the average axial and lateral strain in the middle of the specimen during the discussed phases. Unfortunately, due to trouble with the

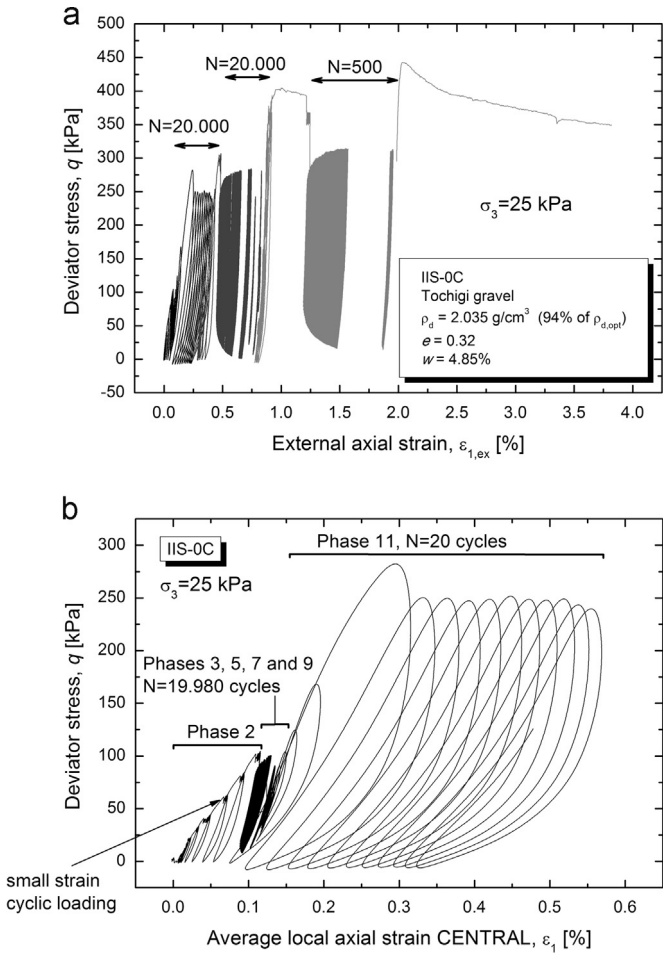

Fig. 6. (a) Overall axial stress–strain relationship and (b) its close-up view up to Phase 11, test IIS-0C.

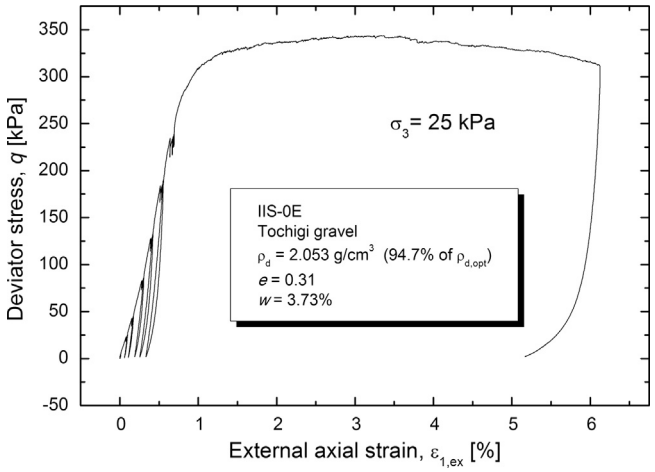

Fig. 7. Overall axial stress–strain relationship, test IIS-0E.

measuring system, the lateral strain was read only from Phase 3 on. It can be seen that the permanent strain caused by the axial load is small compared to the strain due to the increased confinement, except for the strain caused by the initial load cycles (Fig. 13(a)). The lateral strain caused by the increased confinement was almost

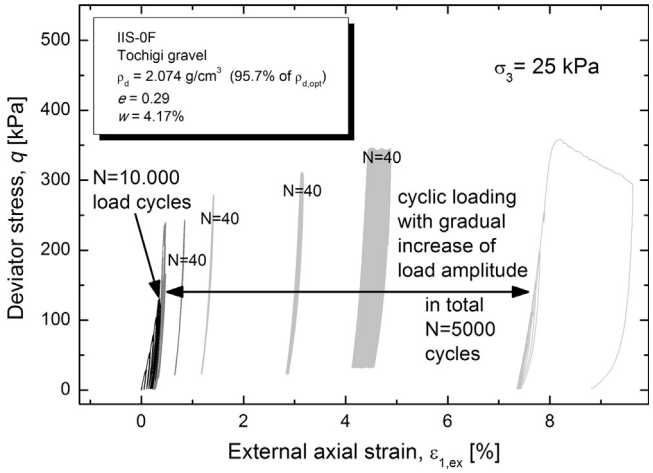

Fig. 8. Overall axial stress–strain relationship, test IIS-0F.

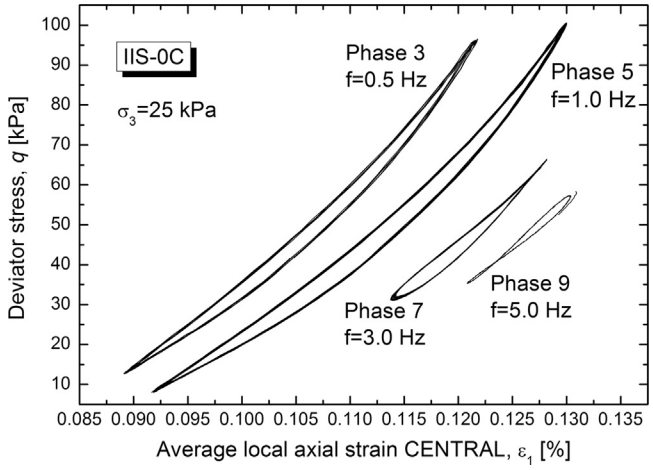

Fig. 9. The effect of loading frequency on the achieved loading amplitude during cyclic loading. The hydraulic actuator was not always able to perform the loading with the desired load amplitude (q=0–100 kPa).

twice as large as the axial one. Due to the increased confinement, the specimen contracted noticeably. During Phases 3–7 (σ_3=10–25 kPa) contraction occurred almost only in the lateral direction, whereas axial strain is caused mostly by the cyclic deviator stress. This might be due to the specimen preparation by vertical compaction. When the confining pressure exceeds 25 kPa, the contraction caused by the confining pressure becomes noticeable also in the vertical direction. A decrease in confining pressure in Phase 13 (75 kPa decreases to 10 kPa) similarly caused the dilation of the specimen, with some plastic strain left (see the dashed line in Fig. 13(b)).

5.2. Stress–strain and volumetric response

It was part of our aim to find the difference between the virgin loading and the loading after a certain amount of preloading. Axial strain ε_1 measured locally in the middle of the specimen versus deviator stress q is presented in Figs. 14 and 15.

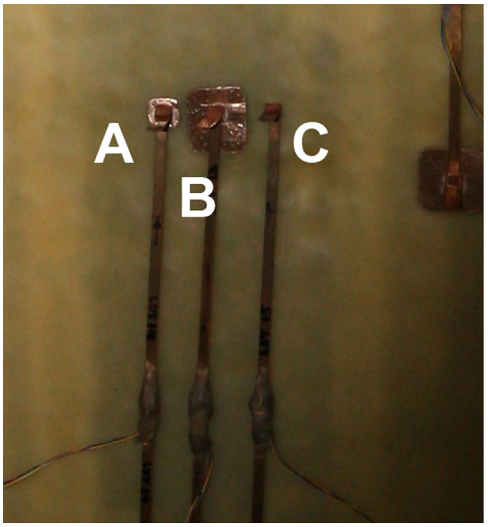

Fig. 10. Three different types of pseudo-hinge attachments.

For reference, the stress–strain response during Phase 2 of test IIS-0E, with monotonic loading up to a certain level of deviator stress, followed by unloading to a deviator stress of zero and then reloading, is presented in Fig. 14(a). The slightly concave shape of the stress–strain relationship during the virgin loading can be initially observed. When the deviator stress exceeds 125 kPa, the shape of the curve becomes convex. Compared to the case with a high confining pressure (e.g., σ_3=490 kPa in AnhDan and Koseki (2004)) a difference can be noticed. The latter exhibits a more pronounced convex shape without any concavity. A similar concave shape during unloading and an almost linear shape of the stress–strain relationship during reloading can be observed in both cases. The volumetric response (Fig. 14(b)) can reasonably explain this phenomenon. The contractive behaviour of the specimen is initially observed at each (re)loading, corresponding to a concave shape of the stress–strain relationship. By contrast, later stages of the loading always exhibit dilative behaviour, corresponding to the convex shape of the stress–strain curve. The overall shape of the stress–strain curve (see Fig. 7) is convex as the specimen generally shows a dilative volumetric response.

20,000 cycles with different stress amplitudes (up to q=100 kPa) were initially applied (up to Phase 9) in test IIS-0C, followed by loading cycles at higher deviator stress levels in Phase 11 (Fig. 6(b)). The specimen showed non-linear almost-elastic behaviour, with a slightly concave shape during reloading at the end of the 20,000 load cycles. When loading at a higher stress level was started (virgin loading), the shape of the stress–strain relationship became slightly convex, exhibiting the additional accumulation of plastic strain. The shape of the (re)loading stress–strain relationship changed from linear to slightly concave again when the deviator stress decreased in the following load cycles.

Fig. 15(a) presents the loading curve in test IIS-0F at a similar amount of previously accumulated axial strain as in the case of test IIS-0C (Fig. 6(b)). The initial 10,000 load cycles with a

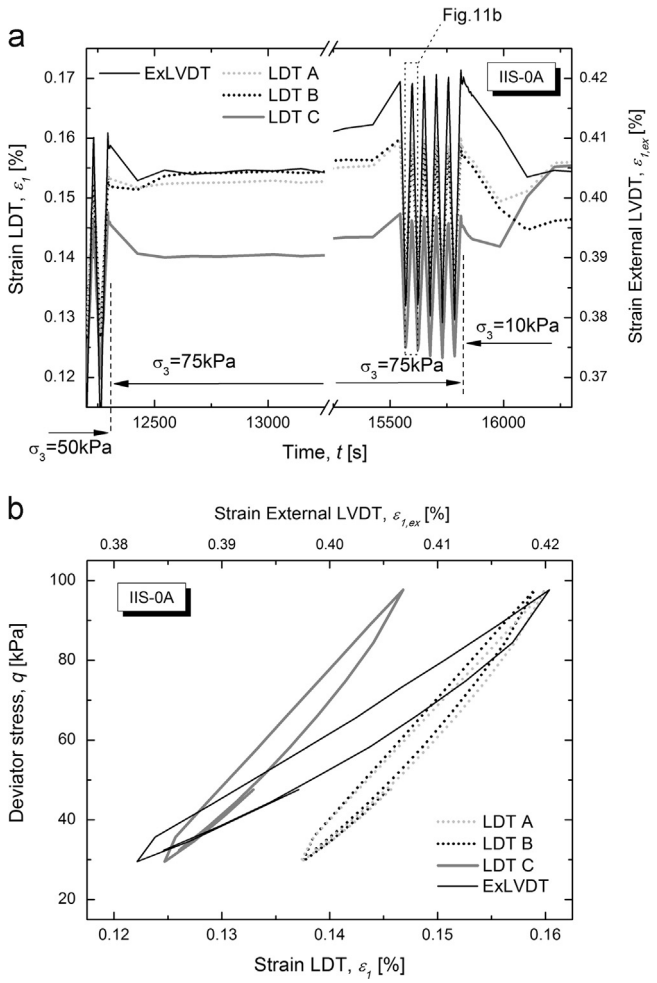

Fig. 11. (a) Axial strain vs. time and (b) deviator stress vs. axial strain (b). The strain was measured locally using three different types of pseudo-hinge attachments and making a comparison to the axial strain measured by an external LVDT.

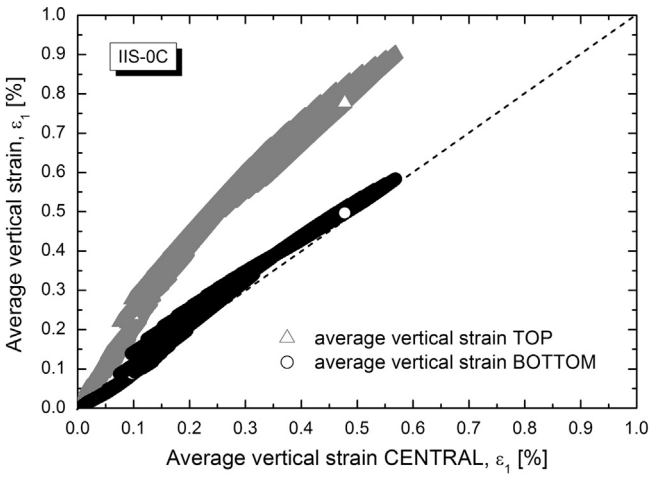

Fig. 12. The typical effect of bedding error on average vertical(axial) strain, test IIS-0C.

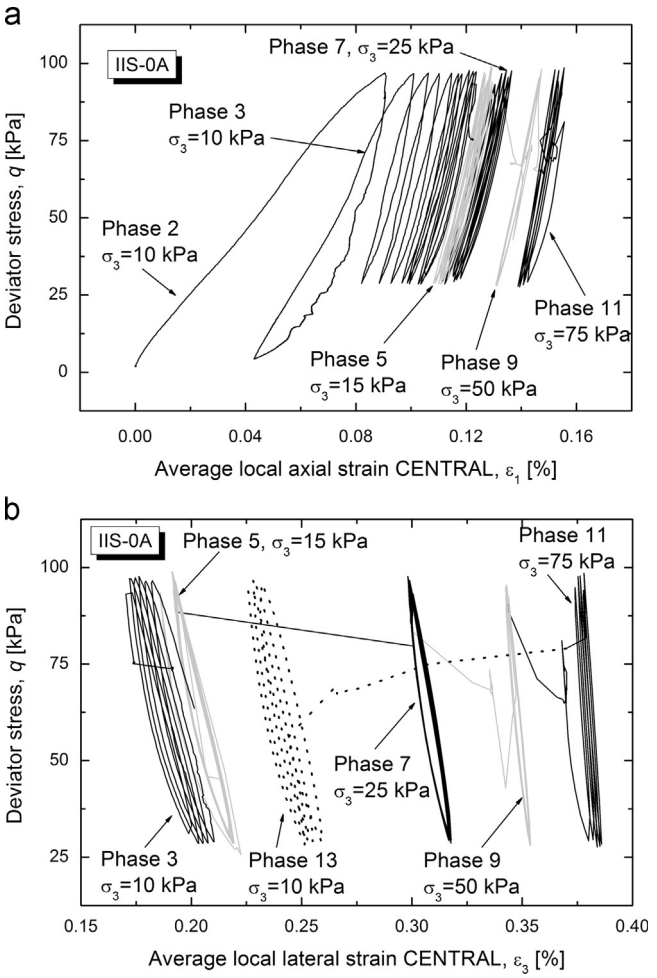

Fig. 13. Close-up view of first few phases of test IIS-0A with gradually increasing confining pressure. (a) Axial and (b) lateral strain was measured by the local LDT at the mid-height of the specimen.

cyclic stress amplitude of 130 kPa (Phase 3) are not shown. The virgin loading from $q=130$ to 230 kPa (Phase 4) exhibited a stress–strain relationship with a convex reloading shape, which later became a concave shape during unloading. Reloading at a smaller load amplitude (Phase 5) resulted initially in a linear-slightly concave shape of the stress–strain relationship. As the number of load cycles increased, the stress–strain curve shape became more concave. The volumetric response (Fig. 15(b)) was very similar to that presented in the reference case (Fig. 14(b)), with a difference in the total volumetric strain, which proves that the specimen contracts due to the large number of load cycles, while it dilates during monotonic compression.

5.3. Effect of large number of load cycles

Fig. 16 compares the stress–strain relationship and volumetric strain resulting from two identical loading patterns in test IIS-0F, before (Phase 2) and after (Phase 4) 10,000 load cycles. The behaviour observed during the 10,000 load cycles is not shown in the figure. Fig. 16(a) presents the large volumetric strain caused by cyclic loading. Noticeable plastic axial strain occurred during cyclic loading (Fig. 16(b)), whereas practically no additional accumulation of plastic strain is observed during the unloading steps after the 10,000 load

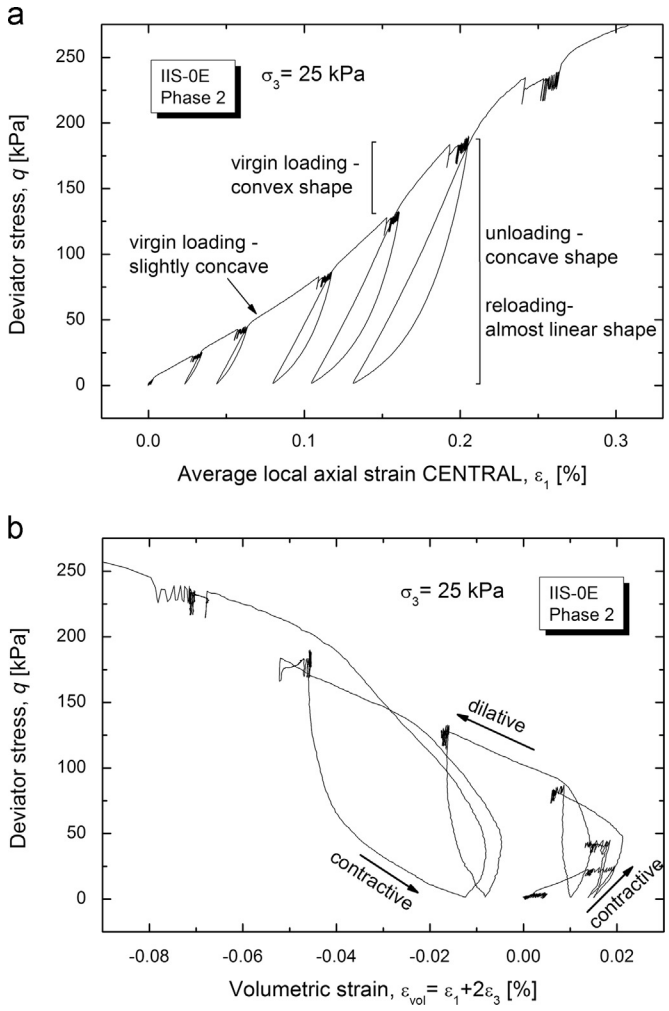

Fig. 14. (a) Reference stress–strain relationship and (b) volumetric response in case of no preloading or large-number cyclic loading, test IIS-0E.

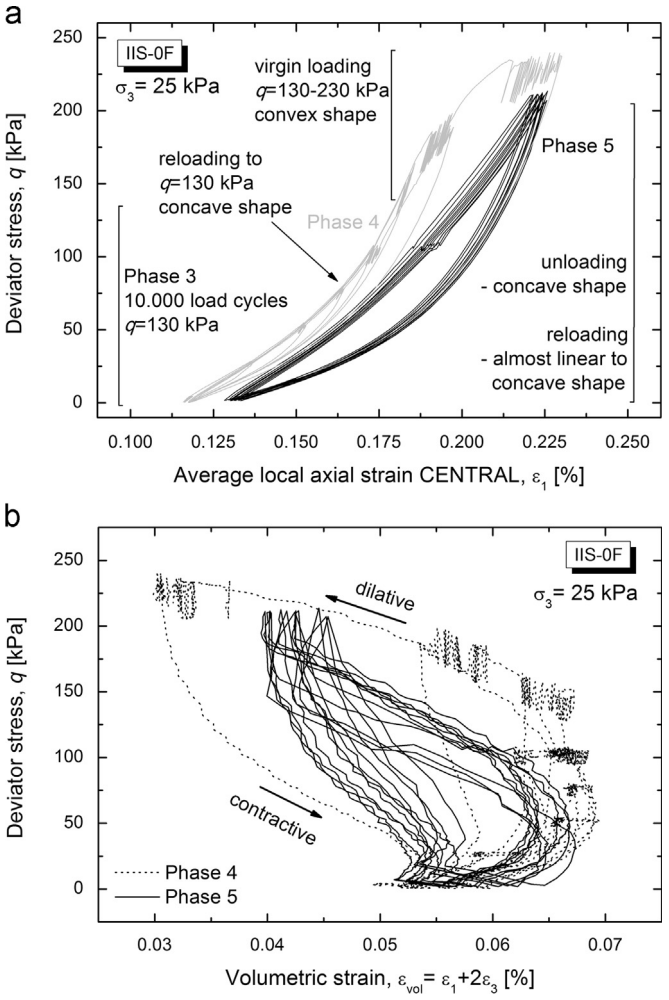

Fig. 15. (a) Typical stress–strain relationship during cyclic loading after preloading and (b) corresponding volumetric response, test IIS-0F.

cycles. The specimen showed stiffer non-linear almost-elastic behaviour after this large number of loading cycles. The development of lateral strain is shown with a dashed line on the left side of Fig. 16(b). A large lateral expansion was observed during the virgin loading, whereas the additional 10,000 load cycles contributed negligibly to the lateral strain. This means that the specimen only densified during a large number of loading cycles and exhibited no lateral expansion.

Further, the tangent Young′s modulus E_{tan}, defined as the slope of the compression stress–strain curve at any specified stress, was analysed in order to describe the behaviour in the plastic region. The dark colour symbols in Fig. 17 denote E_{tan} for the virgin loading (which means the first loading at a specific deviator stress) for two tests (IIS-0E and IIS-0F). The two tests exhibited similar values. Very high values for E_{tan}, approaching quasi-elastic behaviour, can be observed at a very small deviator stress. These values decrease significantly when the stress state enters the plastic region. E_{tan} increases slightly with an increase in the deviator stress, but decreases when the deviator stress approaches the yield condition. The lines are broken several times since unloading and reloading are not included in the analysis of the virgin loading. It can be seen that the E_{tan} values immediately after each reloading are higher, but soon decrease. A similar effect initiated by the strain rate was noted in tests at high levels of confining pressure by AnhDan et al. (2006a).

Light colour symbols (Fig. 17) are used for the cases when the specimen was preloaded (IIS-0E). The tangent stiffness increased noticeably for all deviator stress levels smaller than the one used during preloading. After the 10,000 preloading cycles (IIS-0F), only a slightly higher E_{tan} value (compared to the virgin loading) can be observed at a small deviator stress. The tangent stiffness increased noticeably when the deviator stress increased.

6. Conclusions

Four dense specimens of gravel material were tested at low levels of confining pressure and different deviator stress patterns. The strain was measured locally on the specimens. The present research had two main goals: (1) to modify the existing large-scale triaxial testing device for tests at low levels of confining pressure, and (2) to investigate the deformation

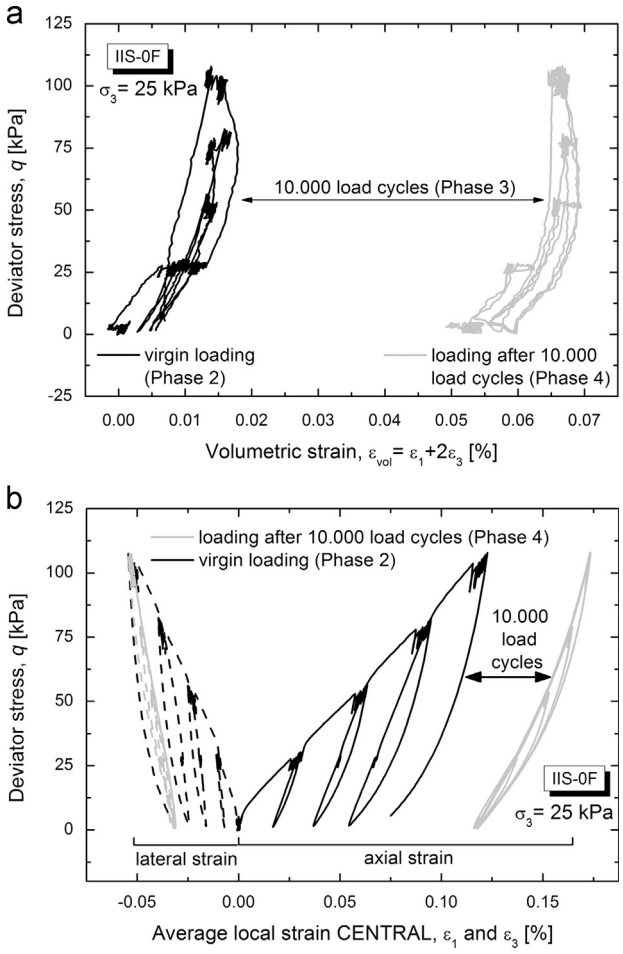

Fig. 16. (a) Volumetric strain and (b) change in stress–strain relationship caused by a large number of load cycles during test IIS-0F. The dashed lines denote the lateral strains. The same loading pattern was used before and after the cyclic loading.

properties of dense gravel material at low levels of confining pressure.

The first two challenges caused by the modification of the testing conditions were the proper attachment of local deformation transducers to the membrane of the specimen, and the elimination of friction between the specimen and the rigid plates of the top cap and the pedestal. Therefore, the use of an extra plate to increase the contact area between the hinge and the membrane, and the use of double lubrication layers at both ends of the specimen were proposed and verified in this research.

Besides confirmation of the proposed solutions, the paper presented the results of loading tests showing similar effects of one-time preloading or loading by a large number of load cycles on the deformation behaviour of specimens. A load amplitude of loading cycles, equal to the current deviator stress, should be used to observe a similar trend. This results in the appearance of the non-linear almost-elastic behaviour of the specimen, with the shape of the stress–strain relationship changing from convex to concave. Similar behaviour was also noticed in the case of previous tests performed under higher levels of confining pressure (AnhDan and Koseki, 2004; Maqbool and Koseki, 2010). When compared to the higher confining pressure test results, differences can be noticed in the case of the virgin loading. While the stress–strain response during the virgin loading exhibited a convex shape without any concavity in the case of high confining pressure, a slightly concave shape can be observed initially in the case of low confining pressure. The volumetric response can reasonably explain the transformation of the shape of the stress–strain curve from convex to concave, and vice versa. It was also found in the research presented here that the contractive behaviour of the specimen corresponds to a concave shape of the stress–strain relationship, and the dilative behaviour corresponds to a convex shape.

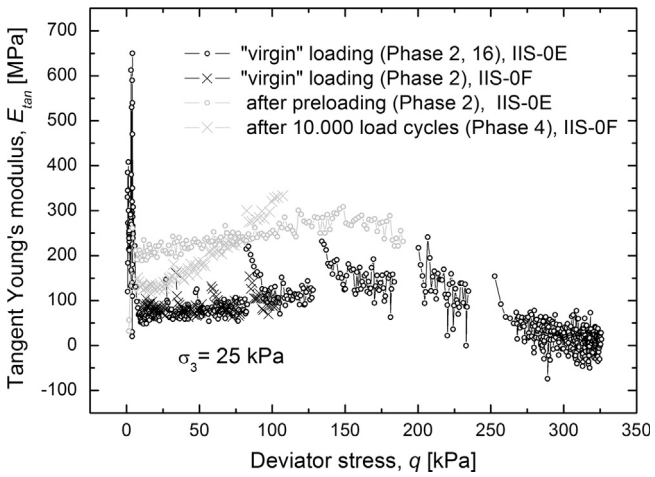

Fig. 17. Effect of preloading history upon the tangent stiffness, tests IIS-0E and IIS-0F.

The laboratory test results prove that preloading causes a noticeable increase in the tangent stiffness of specimens in the case of low confining pressure. The plastic axial strain due to preloading is accompanied by lateral expansion, and thus, results in dilation. On the other hand, a large number of load cycles causes noticeable plastic axial strain accompanied by negligible lateral strain, and thus, densifies the specimen. Compared to the virgin loading, the tangent stiffness is only slightly higher at a low deviator stress after a large number of cyclic loadings, but increases noticeably with an increase in deviator stress. For possible practical implications, although preloading and a large number of cyclic loadings have a similar positive effect on the stiffness characteristics of unbound gravel material exposed to traffic loading, excessive preloading should be avoided as it can cause dilation of the material. It is also to be noted that research performed at high levels of confining pressure suggests a positive effect of the large number of cyclic loads up to a certain threshold of deviator stress amplitude. This threshold, in the case of low levels of confining pressure, should be studied in the future.

Acknowledgements

The authors would like to thank the Japan Society for the Promotion of Science (JSPS) for the financial support of the

first author's postdoctoral research work at the Institute of Industrial Science, University of Tokyo.

References

AnhDan, L.Q., Koseki, J., 2004. Effects of large number of cyclic loading on deformation characteristics of dense granular materials. Soils Found. 44 (3), 115–123.

AnhDan, L.Q., Tatsuoka, F., Koseki, J., 2006a. Viscous effects on the stress–strain behavior of gravelly soil in drained triaxial compression. Geotech. Test. J. 29 (4), 330–340.

AnhDan, L.Q., Koseki, J., Sato, T., 2006b. Evaluation of quasi-elastic properties of gravel using a large-scale true triaxial apparatus. Geotech. Test. J. 29 (5), 374–384.

Erlingsson, S., Magnusdottir, B., 2002. Dynamic triaxial testing of unbound granular base course materials. In: Proceedings of the 6th International Conference on the Bearing Capacity of Roads, Railways and Airfield, Lisbon, pp. 989–1000.

Ezaoui, A., Tatsuoka, F., Sano, Y., Iguchi, Y., Maeda, Y., Sasaki, Y., Duttine, A., 2010. Ageing effects on the yielding characteristics of cement-mixed granular materials. Soils Found. 50 (5), 705–724.

Gomes-Correia, A., Hornych, P., Akou, Y., 1999. Review of models and modelling of unbound granular materials. In: Proceedings of an International Workshop on Modelling and Advanced Testing for Unbound Granular Material, Lisbon, pp. 3–15.

Goto, S., Tatsuoka, F., Shibuya, S., Kim, Y.-S., Sato, T., 1991. A simple gauge for local small strain measurements in the laboratory. Soils Found 31 (1), 169–180.

Goto, S., Park, C.-S., Tatsuoka, F., Molenkamp, F., 1993. Quality of the lubrication layer used in element tests on granular materials. Soils Found. 33 (2), 47–59.

Hoque, E., Tatsuoka, F., Sato, T., 1996. Measuring anisotropic elastic properties of sand using a large triaxial specimen. Geotech. Test. J. ASTM, 19; 411–420.

Inam, A., Tatsuya Ishikawa, T., Miura, S., 2012. Effect of principal stress axis rotation on cyclic plastic deformation characteristics of unsaturated base course material. Soils Found. 52 (3), 465–480.

Maqbool, S., Koseki, J., 2010. Large-scale triaxial tests to study effects of compaction energy and large cyclic loading history on shear behavior of gravel. Soils Found. 50 (5), 633–644.

Momoya, Y., Sekine, E., Tatsuoka, F., 2005. Deformation characteristics of railway roadbed and subgrade under moving-wheel load. Soils Found. 45 (4), 99–118.

Poulos, H.G., Davis, E.H., 1974. Elastic Solutions for Soil and Rock Mechanics. John Wiley & Sons, New York.

Taheri, A., Sasaki, Y., Tatsuoka, F., Watanabe, K., 2012. Strength and deformation characteristics of cement-mixed gravelly soil in multiple-step triaxial compression. Soils Found. 52 (1), 126–145.

Taheri, A., Tatsuoka, F., 2012. Stress–strain relations of cement-mixed gravelly soil from multiple-step triaxial compression test results. Soils Found. 52 (4), 748–766.